# Anomalous statistics of aftershock sequences generated by supershear ruptures

**Pathikrit Bhattacharya,[1] Robert Shcherbakov,[1,2] Kristy F. Tiampo,[1] Lalu Mansinha[1]**

**[1]Department of Earth Sciences, University of Western Ontario, Canada; [2]Department of Physics and Astronomy, University of Western Ontario, Canada**

## Abstract

Most earthquake ruptures propagate with speeds smaller than the Rayleigh wave velocity of the medium. These are called sub-Rayleigh ruptures. However, under suitable conditions, segments of otherwise sub-Rayleigh seismogenic ruptures can occasionally accelerate to speeds higher than the local shear wave velocity, giving rise to so-called supershear ruptures. The occurrence of supershear ruptures is usually associated with a locally higher value of pre-stress on the fault segment compared to the sub-Rayleigh segments of the same fault. Additionally, shear stress changes generated by the supershear rupture are radiated out unattenuated to distances comparable to the depth of rupture instead of rapidly decaying at much smaller distances from the rupture. This leads to aftershocks being distributed away from the fault on the supershear segment. This study attempts to verify whether these pre- and post-seismic stress conditions and the resultant spatial aftershock distributions lead to discernible features in the statistical properties of the aftershock sequences of the earthquakes known to be associated with supershear ruptures. We analyze the Gutenberg-Richter scaling, the modified Omori law and Båth's law for the aftershock sequences of two supershear mainshocks: the 1979 $M_W$ 6.5 Imperial Valley (California) and 2002 $M_W$ 7.9 Denali (Alaska) earthquakes. We observe that the *b*-value is always higher in the supershear zone than the rest of the sequence. We also observe that there is no systematic trend in the exponent of the modified Omori law when comparing the aftershocks in the supershear zone with the rest of the aftershocks. We argue that the *b*-value anomaly can be explained in terms of the off-fault distribution of aftershocks around the supershear segment of the rupture.

## Introduction

An earthquake rupture is called supershear if it propagates stably with a velocity greater than the local shear wave velocity but less than the local dilatational wave velocity for some part of its spatio-temporal history.[1] Most shallow crustal earthquakes occur due to sudden rupturing of the crust along pre-existing fault planes under remote tectonic loading. The growth of mode II ruptures in linear elastic media containing a plane of weakness is a good theoretical analog for this problem. Mode II ruptures are in-plane shear ruptures where the relative sliding of the crack faces is constrained on the crack plane and is perpendicular to the crack front. Theoretical solutions of such models predicted supershear ruptures about thirty years ago[2-4] and their properties were subsequently studied in detail. But observation of supershear ruptures in real earthquakes was not achieved until recently.[5,6] Since direct observation of rupture propagation in the crust is impossible, seismologists have to rely on the ground motion records and seismic inversions to study rupture histories of earthquakes. With recent advancements in both instrumentation as well as computational capabilities, it has become clear that segments of seismogenic ruptures may become supershear in real earthquakes. A combination of instrument records, inversions and field studies have confirmed, with varying degrees of certainty, five large earthquakes where rupture speeds exceeded the local shear wave velocity on some segments of the entire seismogenic rupture: the 1979 $M_W$ 6.5 Imperial Valley (California);[5,6] 1999 $M_W$ 7.6 Izmit (Turkey);[7,8] 1999 $M_W$ 7.2 Duzce (Turkey);[8-10] 2001 $M_W$ 7.8 Kunlunshan (Tibet);[11-13] and 2002 $M_W$ 7.9 Denali (Alaska)[14-16] earthquakes. Apart from these aforementioned events, reports of the rupture velocity exceeding the shear wave velocity on fault patches only a few kilometers long were made for the 1992 $M_W$ 7.3 Landers (California) earthquake.[17,18] The evidence here is less conclusive due to contradictory ground motion records and the fact that rupture speeds over such short distances are poorly resolved. Supershear ruptures are generally associated with unique pre- and post-seismic stress conditions, *e.g.* the requirement of high pre-stress to initiate supershear rupture propagation[19-21] and the transmission of shear stresses within the shear wave mach cones to large distances away from the rupture plane.[1,22] This off-fault stress redistribution and the fact that supershear ruptures are generally seen to occur on frictionally smooth segments of faults lead to the occurrence of aftershocks off the main fault.[23]

The aim of this study was to determine whether this unique pattern of aftershock generation and the pre- and post-seismic stress redistributions affect the aftershock statistics of supershear mainshocks. In particular, we tried to ascertain whether the aftershocks, which occurred near the supershear rupture segment, were statistically different from those, which occurred throughout the rest of the aftershock region. To investigate this, we used the two aftershock sequences with the highest number of reported aftershocks amongst the four listed above: the 1979 $M_W$ 6.5 Imperial Valley (California) and 2002 $M_W$ 7.9 Denali (Alaska) earthquakes. This ensures that we have statistically significant results. To introduce the problem, we first provide a brief description of the physics of supershear ruptures along with descriptions of the two supershear events whose aftershock sequences have been analyzed in this paper. We then describe the statistical parameters we estimate from the sequences along with the details of the methods employed in calculating these features. We estimate the Gutenberg-Richter scaling parameters, modified Omori law parameters and Båth's law for each of the sequences. We also look in detail at the spatial variation of the *b* and *p* values for each of the sequences. Finally, we discuss these results and their implications on the physics of aftershock occurrence.

### Supershear ruptures and aftershock sequences

Earthquakes are generally modeled as shear cracks propagating along planes of weakness

Correspondence: Robert Shcherbakov, Department of Earth Sciences, University of Western Ontario, London, Ontario, N6A 5B7, Canada. E-mail: rshcherb@uwo.ca

Key words: supershear ruptures, Gutenberg-Richter scaling, aftershock statistics, modified Omori law, Båth's law.

Acknowledgments: this work was supported by NSERC Discovery grant 355632-2008 and UWO ADF grant R4203A03 (to PB and RS), the NSERC and Aon Benfield/ICLR Industrial Research Chair in Earthquake Hazard Assessment (to KFT).

Received for publication: 14 November 2011.
Revision received: 5 March 2012.
Accepted for publication: 5 March 2012.


*Research in Geophysics 2012; 2:e6*
*doi:10.4081/rg.2012.e6*

in geological material called faults. Spontaneous ruptures occur when the outward flux of kinetic and strain energy from the nucleation zone overcomes the local fracture energy and the rupture can effectively grow by breaking the intact material lying ahead. As the crack tip is a source of radiation of the elastic waves and the resulting rupture propagation throughout the medium, any perturbation to the propagation of the rupture, and therefore to the rupture velocity, would lead to high frequency ground motions. One example of such rupture speed perturbation, predicted theoretically[2-4] and observed experimentally[24-26] as well as in real earthquakes,[5,14] is the transition of ruptures from sub-Rayleigh to supershear speeds. When observed, this transition implies a set of unique pre- and post-seismic stress and strength conditions on the fault.

## Physics of supershear ruptures

The occurrence of supershear ruptures is generally observed when initially sub-Rayleigh ruptures accelerate to supershear rupture velocities. Using elastodynamic equations of motion under the appropriate initial and boundary conditions, it can be shown that for bilaterally growing mode II ruptures along a plane of weakness in a homogeneous medium, a stress peak travels at speeds higher than the Rayleigh and shear wave velocities ahead of the rupture tip.[2] In other words, the shear stress on the fault begins to increase upon the arrival of the P-phase and continues to grow to a maximum just before the arrival of the S-phase. This local maximum is referred to as the intersonic stress peak.[20] The arrival of the S-phase further relaxes the stress until it reaches a local minimum and then begins to rise again after the arrival of the Rayleigh phase to subsequently reach a singularity at the rupture tip. Under favorable conditions, this intersonic stress peak can cause material to slip across the plane of weakness, causing transient supershear crack growth through the formation of a daughter crack ahead of the main rupture and the S-phase.[3,4] The daughter crack may or may not be connected with the main rupture depending on past rupture history and the peak strength level of the material. Whether or not the rupture ultimately transitions to a supershear propagation velocity depends upon the stability of the daughter crack. This mechanism of sub-Rayleigh to supershear transition is generally known as the Burridge-Andrews mechanism. Theoretical results from rupture dynamics[3,4,20] and experimental evidence (from laboratory samples with a defined plane of weakness)[25] suggest that the pre-requisite for this to happen on a homogeneous fault is that the stress level on the supershear segment of the fault should be closer to the failure strength of the fault patch than to the residual stress level prior to the initiation of rupture on that segment. An additional requirement for the homogeneous fault to host supershear transition is the availability of a long, straight patch of the plane of weakness, which lets the rupture front gather enough energy to become supershear. This requirement of a critical length has also been predicted in theory,[3,4] observed in experiments with pre-cut samples in labs[25] and real earthquakes.[27] Under slip weakening friction, this critical length that the rupture propagates before reaching intersonic speeds has been predicted to be proportional to a length scale arising from the friction law governing the nucleation and stability of the daughter crack and its magnitude is very sensitive to the properties of the friction law used.[20] Finite faults with a width shorter than this critical width do not permit the transition to supershear speeds. Finite faults that are longer than this critical width do allow sub-Rayleigh to intersonic transition (given that other conditions are satisfied) and exhibit transition lengths approximately 0.8 times the transition length on an infinite fault.

Recently, numerical simulations on heterogeneous faults have shown that while the above conditions are sufficient, other physical conditions and mechanisms can lead to supershear transitions as well. The presence of strength or stress heterogeneities can also facilitate the rupture accelerating to speeds higher than the shear wave velocity.[20,21,28] These mechanisms do not require pre-stresses as high as those for the Burridge-Andrews mechanism. When rupture encounters these heterogeneities, stress waves of high amplitudes are produced. If these amplitudes are high enough with respect to the strength of the surrounding material, transient bursts of supershear speeds can be generated.[20] The question as to whether or not the duration of these transients is sufficient to cause a permanent increase in rupture velocity is, however, not easily answered. Additionally, it has been experimentally observed that ruptures can originate as supershear under intersonic loading and propagate as such,[24] but to date this has not been observed in actual earthquakes. Of more interest to us are the post-seismic implications of the supershear ruptures. The formation of supershear ruptures leads to the formation of supershear characteristics in the shear component of stress and particle velocities. These are transmitted along shear mach cones to large distances away from the main rupture. Though the compressional stress dies rapidly away from the main rupture path, the shear stress components travel much further from the fault and remain unattenuated over an off-fault distance on the order of the depth of faulting.[29] The shear stress increase in this region is of the same magnitude as that on the main rupture.[23,29] This is very different from the rapid die off of the shear stress field with off fault distance that is observed in sub-Rayleigh ruptures. Additionally, it has been seen that supershear segments of ruptures show a puzzling lack of high frequency ground motion.[8,11] As the high frequency components of ground motion are primarily the result of frictional or stress heterogeneities on the fault, and as the supershear segment is stress-smoothed, the supershear rupture segments are frictionally smooth as well. If one accepts the barrier model of aftershocks,[30] this precludes the possibility of having aftershocks on the main fault. Such zones of remarkable post-mainshock seismic quiescence have been observed for supershear mainshocks.[23] The aftershocks on supershear segments are systematically located off the main fault on which supershear ruptures are hosted and are observed to activate secondary structures.[23] Therefore, it is of significant interest to analyze whether these unique modes of aftershock occurrence and stress and strength conditions lead to appreciable differences in the statistical properties of aftershocks. This information would give us a better understanding of the physical controls on the statistical properties of aftershocks. Furthermore, it would give us an opportunity to look at the statistical signatures of seismicity as an indirect indicator of rupture behavior on a given fault segment.

## Aftershock sequences considered

As stated above, at least five earthquake ruptures have been inferred to have exceeded the local shear wave velocity on parts of their propagation paths. All of these earthquakes occurred on very mature and well-characterized strike slip fault systems.[27] However, it is not yet clear whether a strike-slip tectonic setting is necessary for supershear rupture speeds to occur. In the present article, we analyze two of these sequences: the 1979 $M_W$ 6.5 Imperial Valley (California) and 2002 $M_W$ 7.9 Denali (Alaska) earthquakes. We undertake statistical analysis of both the aforementioned sequences and try to determine which signals, if any, support the supershear rupture velocity models for these events. These mainshocks and the aftershock sequences are briefly described below.

## The 1979 $M_W$ 6.5 Imperial Valley (California) sequence

The surface faulting of the Imperial Valley earthquake has been studied in detail.[31] Faulting occurred on the Imperial and Brawley faults, rupture on the Brawley fault being triggered by rupture on the Imperial fault. The inferred supershear rupture segment occurred on the Imperial fault[27] (Figure 1A). This segment ends where the Imperial fault intersects with the Brawley fault. The aftershocks consid-

ered are defined as all the seismicity occurring within the spatial box in Figure 1A, between depths of 0-20 km and within the first 183 days of the occurrence of the mainshock. After this period, the seismicity rate tends to fall off to the background level. We use the SCEC catalog (http://www.data.scec.org) for this sequence.

## The 2002 $M_W$ 7.9 Denali (Alaska) sequence

The Denali earthquake produced a surface rupture of about 340 km. Rupture started on a 48 km long north dipping thrust fault, the Sustina Glacier fault, then propagated eastward for nearly 300 km as a strike-slip rupture along the adjacent Denali and Totschunda faults[32] The length of the supershear segment is not precisely known, but modeling of the lone near-fault accelerometer records suggests that the supershear episode began at about 146.5° longitude.[23] A supershear speed of 5.5 km/s and an average rupture velocity of 3.3 km/s give an estimate of about 60 km for the length of the supershear segment (Figure 1B).[15,16,33] The aftershocks considered are defined as all the seismicity occurring within the spatial box in Figure 1B, between depths of 0-20 km and within the first 365 days of the occurrence of the mainshock. We use the AEIC catalog (http://www.aeic.alaska.edu/) for this sequence. We carried out consistent statistical analyzes of both these sequences to examine the signals of interest.

## Statistical methods

The basic statistical properties of any aftershock sequence are described in terms of mainly three empirical statistical laws: the distribution of aftershock magnitudes described by the Gutenberg-Richter (GR) scaling,[34] the decay of aftershock rates with time described by the modified Omori law[35] and the difference between the mainshock and the largest aftershock magnitude described by Båth's law.[36] We investigated all the above three properties of both the aftershock sequences considered and we would suggest that the aftershocks within the supershear zone (the zones enclosed by red boxes in each of the respective maps for the individual sequences) belong to a statistically different population compared to the rest of the aftershocks. To support this we have analyzed the GR scaling and modified Omori law for each of the sequences. Additionally, we have examined the parameters of the GR scaling and modified Omori law inside and outside the supershear zones for both sequences to check whether there is a systematic variation between the parameter values. We also examined the validity of Båth's law for both sequences. The estimation methods used to obtain the relevant parameters are described below.

## Gutenberg-Richter law

The GR scaling is defined as

$$\log_{10} N(\geq m) = a - bm, \quad (1)$$

where $N(\geq m)$ is the number of earthquakes with magnitudes greater or equal to magnitude $m$, and $a$ and $b$ are constants. This relationship holds for global earthquake catalogs and is also applicable to aftershock sequences. Estimation of the $b$-value has been the subject of considerable research and there are various methods. The most statistically appealing of these is the maximum likelihood method[37,38], which gives the estimate of the $b$-value as:

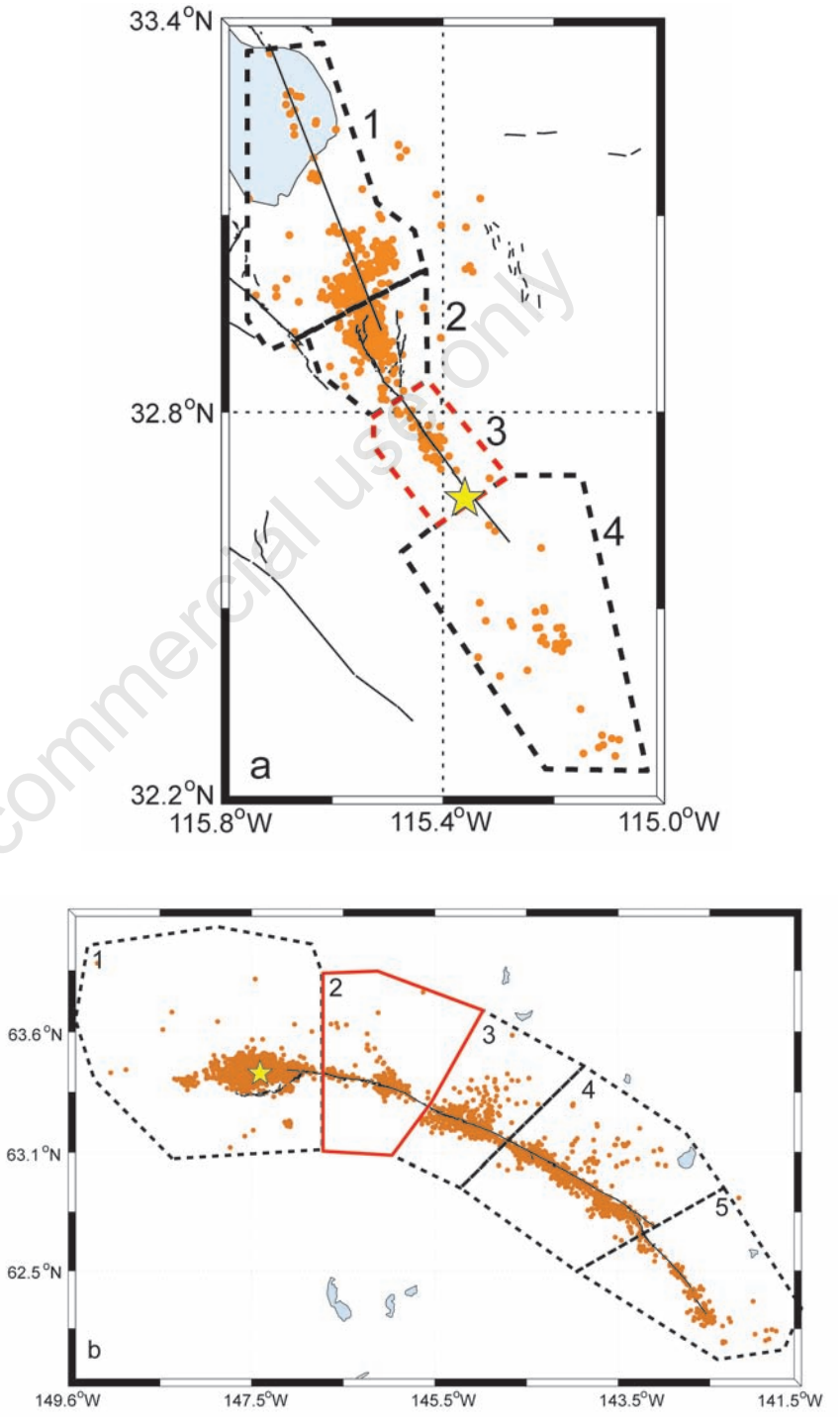


**Figure 1. Spatial distribution of seismicity in the aftershock region considered for (A) the 1979 $M_W$ 6.5 Imperial Valley (California) earthquake (B) the 2002 $M_W$ 7.9 Denali (Alaska) earthquake. Seismic zonation is shown. Red boxes enclose the supershear zones.**

$$\hat{b} = \frac{\log_{10} e}{\bar{m} - m_c + \frac{\Delta m}{2}}, \quad (2)$$

where $\Delta m$ is the magnitude binning width specific for each earthquake catalog, $m_c$ is the completeness magnitude (or the observed minimum magnitude in the catalog above which the GR law can accurately represent the cumulative number of earthquakes larger than a given magnitude) and $\bar{m}$ is the average sample magnitude. To estimate the $b$-value, we use a modified form of Eq. (2) corrected for the fact that magnitudes reported in prevalent seismicity catalogs are binned and not continuous variables:[39–41]

$$\hat{b} = \frac{\log_{10} e}{\Delta m} \ln\left(1 + \frac{\Delta m}{\bar{m} - m_c}\right). \quad (3)$$

This estimate is hereafter called the maximum likelihood (ML) estimate. Plots of the cumulative frequency-magnitude distribution for each of the complete sequences (aftershocks from the whole aftershock region are considered) are given in Figure 2 with ML estimates of the $b$-values in the legend. We have estimated the completeness magnitude for each of the sequences using the Entire Magnitude Range (EMR) method.[42] It is important to correctly estimate the completeness magnitude of these aftershock sequences to ensure that the $b$-value is not biased due to the inclusion of magnitudes smaller than $m_c$. For our statistical analysis, we have had to subdivide our data sets into smaller spatial regions and we use an $m_c$ value that is high enough to be used for all sub-regions and the full aftershock region in an attempt to have least bias due to incorrect $m_c$ estimation on small data sets (Tables 1 and 2). Though this approach leads to higher $m_c$ and hence smaller data sets, this practice is expected to yield more reliable estimates of the $b$-value.

## Modified Omori law

The modified Omori law has the form

$$r(t, \geq m_c) \equiv \frac{dN}{dt} = \frac{1}{\tau\left(1 + t/c\right)^p}, \quad (4)$$

where $t$ is time elapsed since the mainshock, $m_c$ is the lower magnitude cut-off above which earthquakes are taken into account, $\tau$ and $c$ are characteristic times, and $p$ is an exponent specifying how fast the sequence is decaying in time. Thus, this describes the rate of decay of aftershocks with time since the mainshock. We have obtained the values of the parameters by fitting the observed aftershock rates for each of the individual sequences. We obtained $p$, $c(m_c)$ and $\tau(m_c)$ for the 3-year aftershock sequence at different values of $m_c$ using a maximum likelihood estimate of the parameters of the modified Omori relation.[43,44] The errors are obtained by inverting the Fisher information matrix for the computed likelihood function for the modified Omori law. Plots of the aftershock decay rates for each of the complete sequences (events from the whole aftershock region are considered) are given in Figure 3 with the maximum likelihood estimate of the $p$-values in the legend.

## Båth's law

Båth's law is defined as

$$\Delta\bar{m}_{obs} = \bar{m}_{ms} - \bar{m}_{obs}, \quad (5)$$

where $m_{ms}$ is the magnitude of the mainshock and $m_{obs}$ is the magnitude of the largest recorded aftershock in the catalog. The averaging is done over a large number of aftershock sequences. In general, $\Delta\bar{m}_{obs}$ considered to be a constant, $\Delta\bar{m}_{obs} \approx 1.2$, independent of the magnitude of the mainshock.[36] It should be noted that Båth's law is a statistical statement ($\Delta\bar{m}_{obs} \approx 1.2$, only when we average over numerous aftershock sequences) and does not strictly apply to individual aftershock sequences. The difference $\Delta m$ can be evaluated in a manner consistent with the GR scaling, rather than from the catalog itself, as it is possible that the largest magnitude aftershock is yet to occur. To differentiate this from the observed difference between the maximum aftershock magnitude and the mainshock magnitude, $\Delta m_{obs}$, we call this difference $\Delta m_{inf}$. We attempt to infer the largest aftershock magnitude from the GR law and to fit it into the standard picture of Båth's law in order to evaluate both the GR law and Båth's law within a common framework.[45] To achieve this, we set $N\ (\geq m) = 1$ in the Gutenberg-Richter scaling law to obtain

$$a = b\mathrm{m}_{inf} \quad (6)$$

where $m_{inf}$ represents the magnitude of the largest inferred aftershock. In general, $\Delta\bar{m}_{inf} = \bar{m}_{ms} - \bar{m}_{inf} \approx 1.0$. This will be referred to as the modified Båth's law. For example, the intersection of the fit line and the line $N = 1$ gives us the value of $m_{inf} = 6.64$ for the Denali sequence and thus, $\Delta m_{inf} = 1.26$ (Table 2). However, $\Delta m_{obs} = 2.1$ is a larger value, obtained using the observed maximum aftershock magnitude and implying that the largest magnitude aftershock expected (in agreement with the GR scaling) has not yet been observed



**Table 1. The *b*- and *p*-values corresponding to the spatially segmented seismicity maps in Figure 1. The numbering of the zones is the same as in Figure 1. The zone 3 for Imperial Valley and zone 2 for Denali are the ones inferred to have hosted the supershear segments of the corresponding ruptures. The *b*-value in the supershear zone is observed to be always higher than the other segments. There is no such systematic variation in the *p*-value.**

| Imperial valley | | | Denali | | |
|---|---|---|---|---|---|
| Zone | *b*-value | *p*-value | Zone | *b*-value | *p*-value |
| 1 | 0.80±0.13 | 1.85±0.31 | 1 | 0.93±0.07 | 0.99±0.06 |
| 2 | 0.83±0.11 | 1.72±0.21 | 2 | 1.02±0.16 | 1.40±0.25 |
| 3 | 1.34±0.46 | 1.30±0.33 | 3 | 0.71±0.08 | 1.19±0.11 |
| 4 | 0.97±0.38 | 1.59±1.19 | 4 | 0.75±0.07 | 1.33±0.12 |
| 5 | | | 5 | 0.67±0.14 | 1.39±0.30 |

**Table 2. The *b*-values and corresponding results of the significance tests for both the aftershock sequence considered. $b_{SZ}$ is the *b*-value inside the supershear zone (inside the respective red bound boxes in the maps), $b_{RZ}$ is the *b*-value in the rest of the aftershock region. Errors in *b*-values are given at 98% confidence level. Column *P* reports the probability values while column $P_{95}$ gives the significance test results with 1 implying the null hypothesis is rejected at 95%. *N* is the total number of aftershocks in the full data set above $m_c$. Note that the *b*-value inside the supershear zone is systematically higher than the rest of the aftershock region and this difference is significant at 95%.**

| Event | $m_c$ | $N$ | $b_{SZ}$ | $b_{RZ}$ | $P$ | $P_{95}$ | $p_{SZ}$ | $p_{RZ}$ | $\Delta m_{obs}$ | $\Delta m_{inf}$ |
|---|---|---|---|---|---|---|---|---|---|---|
| Imperial Valey | 2.50 | 599 | 1.34±0.46 | 0.84±0.08 | 0.0003 | 1 | 1.30±0.33 | 1.57±0.13 | 0.70 | 0.78 |
| Denali | 2.50 | 2530 | 1.02±0.16 | 0.81±0.04 | 0.0013 | 1 | 1.4±0.25 | 1.13±0.05 | 2.10 | 1.24 |

in the sequence.

## Data analysis and results

We estimated the frequency-magnitude statistics and aftershock decay rates for each of the full sequences mentioned above, for all the aftershocks observed in the respective aftershock regions over the respective time intervals (Figures 2 and 3). We then segmented both the aftershock regions into several smaller zones (Figure 1) to determine whether the seismicity in the supershear zones for the above sequences exhibited any *b*- or *p*-value anomalies. This zonation was based on the spatial positions of seismicity clusters and local geology and tectonics. However, for each sequence, one of these zones was constructed such that it contained the inferred supershear segment of the corresponding rupture (Figure 1). The extent of the supershear segments as inferred from kinematic and/or dynamic inversions of seismological records in the literature for Imperial Valley and Denali are clearly demarcated[23,27] and we use these extents in this study. We estimated the *b*- and *p*-values for each segment for both the sequences (Table 1 and Figure 4). Table 1 shows that the *b*-values in the supershear zones for each of the sequences are higher than those for the other segments. There is no such systematic variation in the *p*-values. Using this approach we were able to demarcate the spatial extent of the high *b*-value zone, which is the same as the supershear zone. To further enhance the signal observed in the *b*-values we then re-segmented the seismicity into the supershear zone (hereafter called SZ) and the rest of the aftershock zone (hereafter called RZ). We then re-estimated the parameters of the GR scaling and modified the Omori law inside and outside the SZ for the two sequences to check whether there was a systematic statistical variation in the values of the parameters between the two zones (Table 2 and Figure 5).

The most striking feature of the aftershock sequences of supershear mainshocks is the spatial heterogeneity of the *b*-values. In both sequences, we found that the *b*-value inside the SZ is higher than the *b*-value within the RZ (Table 2). An important issue with estimating *b*-values is probably the correct estimation of the completeness magnitude of the aftershock sequence and ensuring that the *b*-value is not biased due to the inclusion of magnitudes smaller than $m_c$ in the sample being used for estimation. As described above, we only use magnitudes higher than the $m_c$ value for the estimation of the *b*-value. But, the completeness magnitude of aftershock sequences can be a complicated function of time. Until now our results were based on the assumption that the entire aftershock sequence has the same completeness magnitude at all times. This assumption may lead to biased estimates of the *b*-value for aftershock sequences. In the case of aftershocks, the major contributing factor is the fact that there is a lack of reliable data immediately after a mainshock. The detailed analysis of aftershock sequence waveforms reveals that a significant number of early events are missing in existing catalogs.[46,47] This is generally ascribed to the lower sensitivity of recording instruments to smaller events in the wake of a large event and its large aftershocks. This leads to very high completeness magnitudes early in an aftershock sequence. There is a subsequent decrease in the completeness magnitude of aftershock sequences with increasing time since the mainshock until it reaches a stable value. We

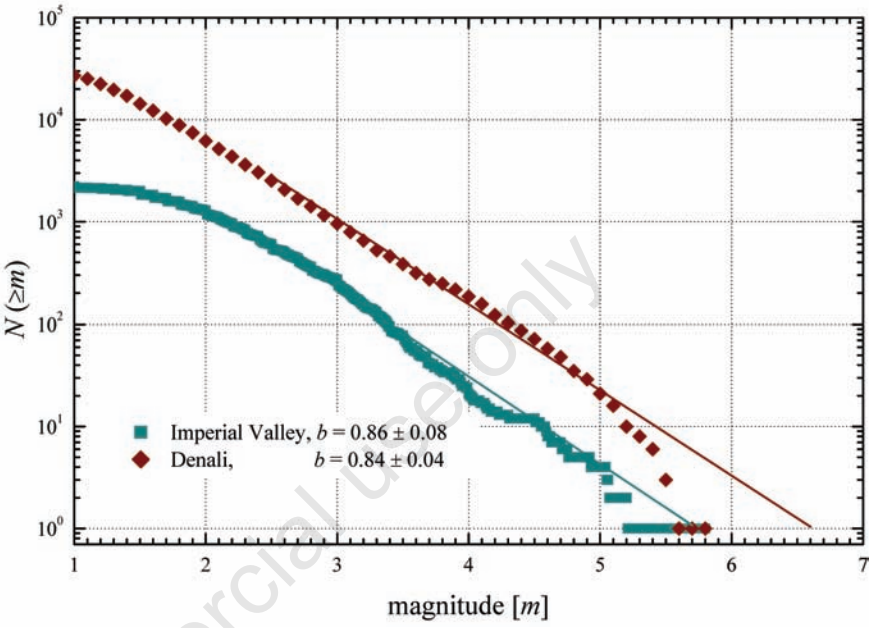


**Figure 2. Frequency-magnitude plots for the sequences considered in the text. The *b*-values reported in the legend are for the full sequences (the whole aftershock region with $T_{cut}$ = 0 days) estimated using the TM method. Errors are reported at the 98% confidence level.**

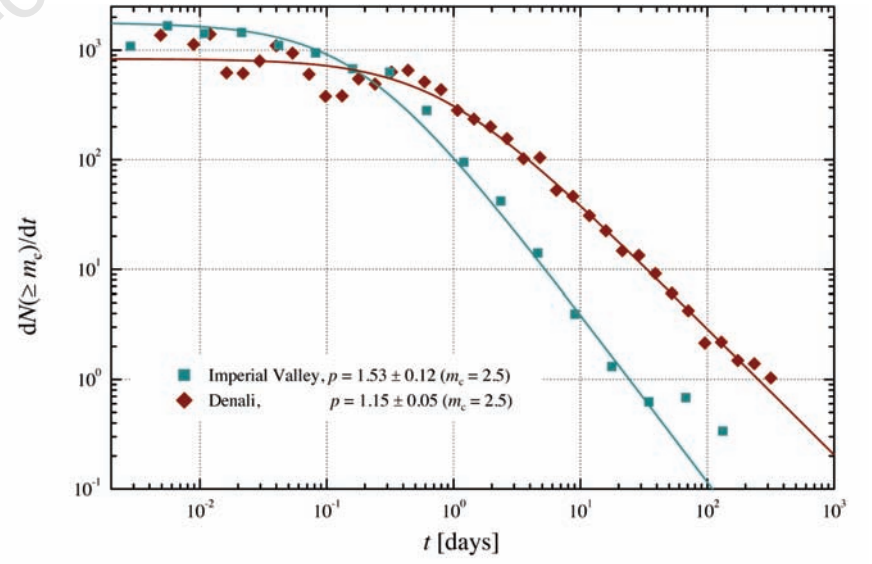


**Figure 3. The rate of the decay of aftershocks for the sequences considered. Solid curves show the modified Omori law with the parameters estimated using the maximum likelihood method. The legend shows the respective *p*-values with 98% confidence intervals.**

calculated the variation of $m_c$ with time using the EMR method.[42] A commonly used method to remove the effect of these early variations in $m_c$, on the estimation of $b$-values, is to introduce a time truncation of the aftershock sequence. In other words, we choose a starting time value $T_{cut}$ days and remove all aftershocks occurring before this value. This choice of $T_{cut}$ is dictated by the variation of $m_c$ with time. We choose a $T_{cut}$ which minimizes the early variability in $m_c$ immediately after the mainshock but does not significantly worsen the statistics due to event removal. In our case, we choose $T_{cut}$ = 1 day as the optimum value (after the first 1 day the fluctuations in $m_c$ are small for both sequences) and use this for both the Imperial Valley as well as Denali sequences. We know the $m_c$ after $T_{cut}$ = 1 day from the time variation of $m_c$ obtained for each of the aftershock data sets using the EMR method within shifting time windows. We use the $m_c$ estimated at $T_{cut}$ = 1 day using the EMR method as the minimum magnitude for estimation of the $b$-value (Table 3) to remove the effect of possible bias by choosing too low an $m_c$. Re-estimation of the parameters from the $T_{cut}$ = 1 day sequences removes possible completeness artifacts in the estimation procedure. The results of this re-estimation are shown in Table 3. Again we obtain the same trend, i.e. the $b$-value inside the SZ is systematically higher than the $b$-values in the RZ for each of the sequences.

We performed significance tests to confirm the statistical significance of the differences observed in the estimated $b$-values. We used a re-sampling version of Fisher's permutation test[48] at the 95% confidence level (Tables 2 and 3). For $T_{cut}$ = 0 days, the differences in the $b$-values between the two zones are significant at the 95% confidence level for both Imperial Valley and Denali sequences. For $T_{cut}$ = 1 day, we obtain similar results for the significance tests (Table 3), although the difference between $b$-values inside the SZ and RZ for Imperial Valley is now statistically significant only at 93%. This very clearly demonstrates that there is a statistical difference between these two populations of aftershocks and that this difference is of high statistical significance.

The estimation of the $p$-value of the modified Omori law does not reveal a clear trend (Table 2). The $p$-values are generally high both inside and outside the SZ. But for the Denali sequence the $p$-value in the SZ is higher while for Imperial Valley it is lower than the $p$-value obtained in the RZ. As there is a clear lack of a systematic signal, we conclude that the $p$-values show no systematic spatial heterogeneity and further significance tests were used.

The third feature studied was the difference

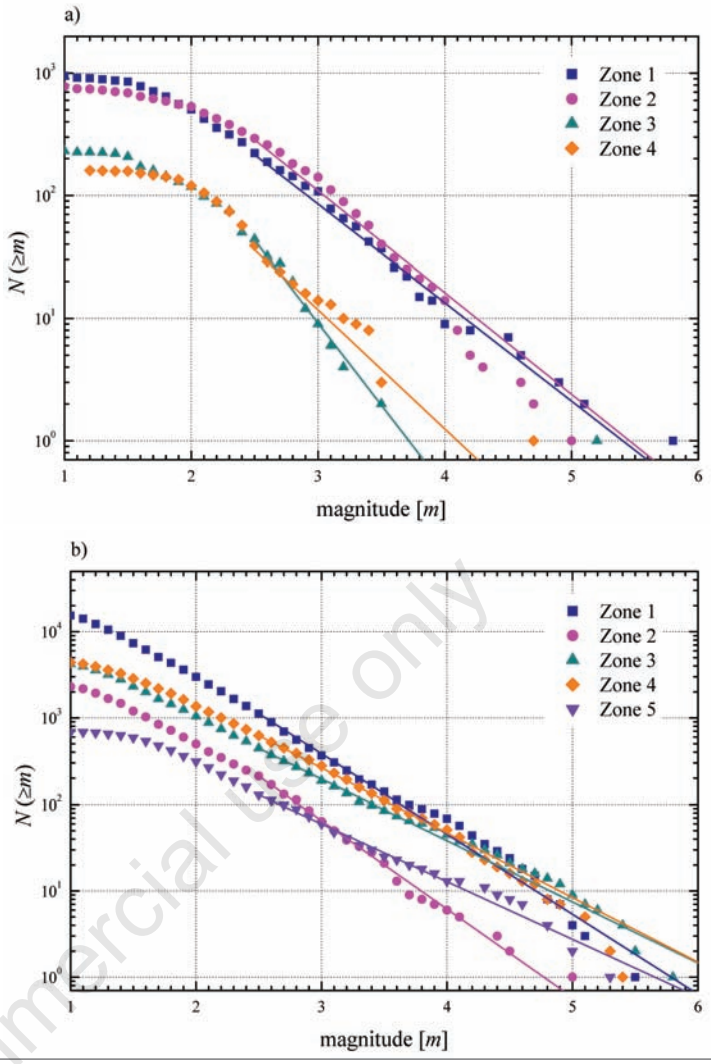


**Figure 4. The frequency-magnitude plots for the subregions of the (A) Imperial Valley aftershocks and (B) Denali aftershocks considered in the text (see Table 1). Solid lines show the GR law fits for the $b$-values given in Table 1.**

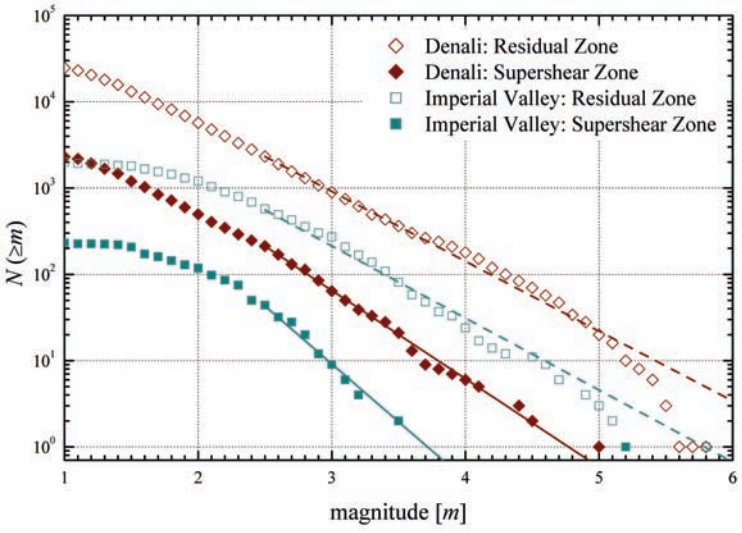


**Figure 5. The frequency-magnitude plots for the supershear zone (SZ) and residual zone (RZ) of the Denali and Imperial Valley aftershock sequences as considered in the text (see Table 2). The solid lines show the GR law fits for the $b$-values given in Table 2 for SZ and the dashed lines show the same for RZ.**

between the magnitudes of the mainshock and the largest aftershock as determined from Båth's law. Table 4 shows the results of this analysis. The original form of Båth's law ($\Delta m_{obs}$ = 1.4) is slightly larger than the value expected from averages over large data sets ($\Delta m_{obs}$ = 1.2). It thus appears that the largest magnitude aftershock is smaller in magnitude than that to be expected from a mainshock of the given size. This is consistent with previous reports of the largest aftershock magnitude being smaller than that expected from Båth's law in aftershock sequences generated by supershear events.[23] However, the modified form ($\Delta\overline{m}_{inf}$ = 1.0) gives the value one would expect by averaging over a large data set for normal, sub-Rayleigh earthquakes. One must recognize that here we are examining only two events and probably there is a strong sampling bias. So this analysis is really for the sake of completeness and it is not immediately clear whether any major physical inferences could be drawn from these values.

## Discussion

### Physical implications of the statistical features

Two main features of this statistical analysis of supershear ruptures are striking: i) the *b*-value is higher in the SZ than in the RZ which points to the fact there is a relative reduction in the number of large magnitude aftershocks with respect to the number of small magnitude aftershocks in the SZ; ii) the decay rate of aftershocks in time, controlled by the *p*-value, shows no systematic variation. Result i) is of particular interest to us and we shall call this the b value anomaly. Result ii) shows that the temporal decay of aftershock occurrence rate follows no particular correlation with the spatial location of the supershear rupture segment.

### The *b*-value anomaly

One could argue that the very large stress drops associated with the occurrence of supershear ruptures on the SZ segment may spatially smooth out the stress profile on this part of the rupture. For a stress drop $\Delta\tau$ accompanied by a co-seismic slip $\delta$ on a fault of length scale l and rigidity $\mu$, on average, one can write:

$$\frac{\Delta\tau}{\delta} \approx \frac{\mu}{l}. \qquad (7)$$

For a fault with constant rigidity throughout, the stress drop would scale as the slip. In regions of high stress drop, or stress release, we should, therefore, also have large co-seismic slip. Thus the supershear segment would also experience the largest co-seismic slip. It has been observed, that the *b*-value is high for populations of aftershocks in regions of large slip on the rupture plane for *normal* (here implying ruptures with sub-Rayleigh velocities) earthquakes.[49] In particular, it has been observed that aftershocks located on a patch of the rupture plane that has experienced large co-seismic slip exhibit a higher *b*-value than the regional trend while the seismicity on adjacent patches which have experienced smaller or no slip exhibit little to no change in the *b*-value.[49] From such a standpoint, it is relatively intuitive to conclude that the aftershocks in the SZ exhibit the highest *b*-value as they occurred on the rupture segment that experienced the largest co-seismic slip. One could additionally conclude that this is the same behavior one expects from aftershocks related to sub-Rayleigh ruptures and, therefore, in this aspect, supershear ruptures are no different from sub-Rayleigh ones. But it is crucial to recognize that this argument applies only to aftershocks that occurred on the main rupture plane. Unfortunately, in the case of supershear earthquakes, aftershocks are preferentially distributed away from the segment of the main fault with the largest co-seismic slip[23,27] and, therefore, the above explanation cannot fully resolve the *b*-value anomaly.

In such a scenario, a very large fraction of the aftershocks in the SZ are occurring on material that has not yet slipped and, therefore, the pre-stress on this material has not been released. After the mainshock has released most of the pre-stress on the main fault, the off-fault pre-stress in SZ can be higher, equal to or lower than the pre-seismic stress loading on the fault. However, in the absence of slipping, there is no reason to believe that the off-fault pre-stress was lower than the regional pre-stress value in the SZ. Rather, as the supershear segment is expected to experience a higher pre-stress than the rest of the fault, the off-fault pre-stress might be higher than the regional tectonic loading in the SZ. Nevertheless, we will consider the more general case and strive to argue that neither a higher than regional nor a regional pre-stress level on the off-fault region in the SZ can explain the *b*-value anomaly.

It has been suggested that the *b*-value might be closely related to stress regimes across fault zones.[50-53] There exists a hypothesis that as the confining pressure increases with depth, the *b*-value is expected to decrease whereas the average earthquake magnitude is expected to increase. Statistical analysis of several earthquake catalogs have yielded mixed results with some authors claiming validation of the hypothesis[52,54] while on the other hand others consider the significance tests used in these validations biased towards the rejection of the null hypothesis.[48] It can, however, be analytically shown under simplifying but reasonable assumptions that the *b*-value should vary with changes in the pre-stress level.[50] To show this, we shall basically follow the analysis given by Scholz[50] and argue that neither a higher nor a



**Table 3. The re-estimation of the *b*-values with $T_{cut}$ = 1 day. All symbols are the same as in Table 1 except that they are now evaluated for the sequences with all the aftershocks occurring within the first day removed. Errors are reported at 98% confidence level. The value of mc after 1 day is obtained from the time variation of $m_c$ evaluated using the Entire Magnitude Range method. Column *P* reports the probability values while column $P_{95}$ gives the significance test results with 1 implying the null hypothesis is rejected at 95%. We see the same statistical trends as in Table 2. The only difference is that $b_{SZ}$ and $b_{RZ}$ are no longer statistically different at 95% confidence level for the Imperial Valley sequence.**

| Event | $m_c$ (after 1 day) | $b_{SZ}$ | $b_{RZ}$ | *P* | $P_{95}$ | *N* |
|---|---|---|---|---|---|---|
| Imperial valley | 2.10±0.16 | 1.32±0.37 | 1.08±0.12 | 0.0633 | 0 | 537 |
| Denali | 2.50±0.05 | 1.15±0.20 | 0.96±0.05 | 0.0177 | 1 | 2002 |

**Table 4. The *b*-values in a narrow zone containing the rupture (*b*rupt) compared to the *b*-values outside this narrow zone (*b*out). This analysis has been made on the full rupture as well as only on the supershear segment (see Figure 9). Column *P* reports the probability values while $P_{95}$ shows the significance test results for the difference between $b_{rupt}$ and $b_{out}$.**

| | Full | | | | Supershear | | | |
|---|---|---|---|---|---|---|---|---|
| Event | $b_{rupt}$ | $b_{out}$ | *P* | $P_{95}$ | $b_{rupt}$ | $b_{out}$ | *P* | $P_{95}$ |
| Imperial valley | 0.87±0.13 | 0.85±0.11 | 0.7357 | 0 | 1.05±0.56 | 1.73±0.82 | 0.2393 | 0 |
| Denali | 0.84±0.09 | 0.82±0.04 | 0.1283 | 0 | 1.00±0.25 | 1.05±0.22 | 0.1337 | 0 |

regional off-fault pre-stress loading in the SZ can provide a physical explanation of the *b*-value anomaly. We shall then divert from this argument, use the same mathematical construct as given by Scholz,[50] and give a more valid alternative physical explanation of the *b*-value maximum in the SZ in terms of variation in material strength.

Scholz[50] set up a probabilistic model to analyze the stress distribution in a heterogeneous material body subjected to an average uniform applied stress, $\tau_0$. Due to the presence of elastic and structural inhomogeneities such as defects, the local stress at a point, $\tau$, will vary about this average in some complex way. As it is extremely difficult to estimate the deterministic mathematical description of this stress field, assuming that the length scale of the inhomogeneities is much smaller than the scale of the body itself, the local stress $\tau$ can be thought of as a random variable. Under this premise, let us consider the following statistical model: the conditional probability distribution that in a given small area anywhere within the whole sample (small enough to have uniform stress within it) the local stress is $\tau$, given the mean stress (or the pre-stress) is $\tau_0$, will be given by $f(\tau|\tau_0)$. The general shape of $f(\tau|\tau_0)$ is expected to be something close to the distribution in Figure 6 but there may be other shapes depending on the spatial extent of the inhomogeneities in the medium.

However, the following analysis holds independent of the shape. Let the strength of the material of the small region with stress $\tau$ be *S*. Therefore, the probability that the given small region will develop a fracture is given by:

$$F(S|\tau_0) = \int_{\tau \geq S}^{\infty} f(\tau|\tau_0) d\tau \quad (8)$$

and is shown by the shaded portion under the graph in Figure 6.

The value of $f(S|\tau_0)$ is an increasing function of $\tau_0$ given constant *S* or a decreasing function of S given constant $\tau_0$. According to Eq. (8), the probability that a crack will occur within a given region is constant and depends only on the strength and the average pre-stress. More precisely, the probability that a crack will grow to an area *A* and stop as it expands from an area *A* to an area *A*+*dA* is given by the following probabilistic model:[50]

$$g(A)dA = \frac{1 - F(S|\tau_0)}{A} dA. \quad (9)$$

Since the definition of $F(S|\tau_0)$ requires the existence of a fracture, Eq. (9) implies that the existence of a fracture increases the likelihood of fracture growth in the surrounding region or

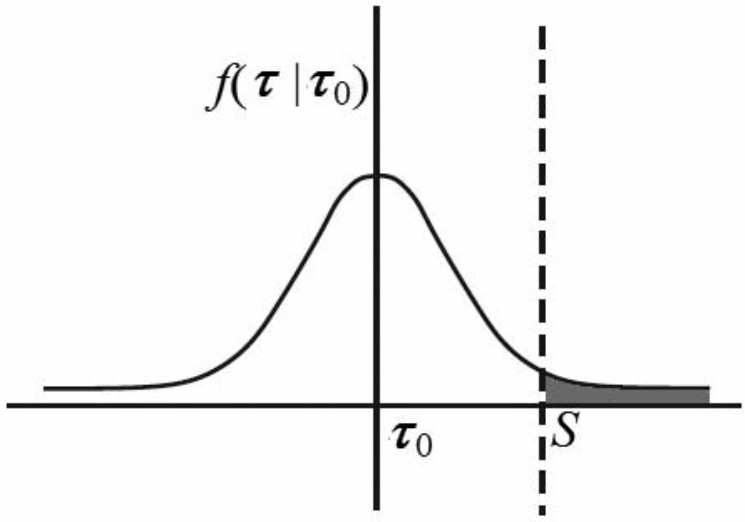


**Figure 6. A hypothetical shape of the function $f(\tau|\tau_0)$ with the parameters the pre-stress $\tau_0$ and the material strength *S*. The gray shaded area shows the domain of integration for the calculation of $F(S|\tau_0)$**

in other words fracturing weakens the surrounding material. Additionally, the larger the fracture is, the larger the possibility of its growth. These two properties capture the essence of the macroscopic properties of fractures. If one defines the number of fractures of an area within the range *A* to *A*+*dA* as $n(A)$, then the cumulative number of fractures in the medium with area larger than A is given by:

$$N(A) = \int_{A}^{\infty} n(A')dA'. \quad (10)$$

As $g(A)dA$ in Eq. (9) represents the probability of occurrence of a crack of area A to A+dA amongst all cracks of area of at least *A*, using the definition of $N(A)$ from Eq. (10) one can write:

$$g(A)dA = \frac{\Pr(\text{area} \leq A + da \cap \text{area} \geq A)}{\Pr(\text{area} \geq A)} =$$

$$\frac{n(A)}{N(A)} dA = -\frac{dN(A)}{N(A)} \quad (11)$$

From Eqs. (9) and (11), it can be readily shown that:[50]

$$[1 - F(S|\tau_0)] d(\log A) = -d[\log N(A)]. \quad (12)$$

One can simplify Eq. (12) to finally obtain:

$$N(A) = A^{-[1-F(S|\tau_0)]}. \quad (13)$$

It is intuitive to understand that, because seismic energy released is related to fracture area, the exponent in the power law in Eq. (13) is related to the *b*-value. In fact, it can be shown clearly that the relationship is:[50]

$$b = \frac{2\gamma}{3}[1 - F(S|\tau_0)] \quad (14)$$

under the assumption that we have narrow, penny shaped cracks in a spherical volume and that cracks of different sizes are similar in shape. Here, $\gamma$ is an empirical constant. Therefore, increase in pre-stress decreases the *b*-value given constant material strength. Scholz showed in his paper that this holds for rock microfracturing in general.[50] It has been shown that this result also holds for earthquake ruptures as well.[53] In particular, the *b*-value varies systematically for different types of faulting with normal faulting events having the highest *b*-values, thrust events the lowest and strike-slip events intermediate values.[53] As thrust faults are generally under higher stress than normal faults, it can, therefore, be inferred that *b*-values depends inversely on differential stress.[53] So, in addition to the debated observations of variations of the *b*-value with depth, our existing knowledge of *b*-values and their dependence on stress leads to the understanding that higher pre-stress regimes should lead to lower *b*-values.

According to Eq. (14), the *b*-value inside the SZ should have been smaller than that in the

RZ if the off-fault pre-stress in SZ was higher than the regional pre-stress experienced by RZ. On the other hand, if the off-fault pre-stress in SZ was close to the regional pre-stress we should not have observed a clear maximum in the *b*-value in the SZ if one accepts that the maximum stress release and the pre-stress are the dominant controlling factors on the *b*-value. This indicates that the *b*-value anomaly is controlled by some other physical factor. We argue that it is probably the preferential off-fault distribution of aftershocks in the supershear zone that creates the *b*-value anomaly.

This view is easily confirmed if one studies Eq. (14). The *b*-value is a decreasing function of $F(S|\tau_0)$. This fact, as stated above, was used[50] to argue that as pre-stress increased, $F(S|\tau_0)$ increased and the *b*-value decreased. But, by the same token, $F(S|\tau_0)$ is also a decreasing function of the strength $S$ of the material. So, if fractures occur on stronger patches of material then the resultant *b*-values will be larger than those observed for fractures on weaker material. The aftershocks in the supershear zone are systematically located off the relatively quiescent main fault segment and hence occur on stronger material, while in the rest of the aftershock zone, most aftershocks occur on or very close to the main rupture. This made $F(S|\tau_0)$ smaller for these aftershocks and hence leads to a larger *b*-value. But as stated before, this analysis does not strictly apply to aftershocks and hence cannot be claimed as the only viable physical cause. It also remains unclear whether the opposing effect of the higher pre-stress on the b value, in case the off-fault region hosting the aftershocks in the SZ was also at the same high pre-stress as the supershear segment of the rupture, can cancel out the effect of the higher strength. It seems that for the two cases studied here, the increasing effects of the strength on the *b*-value are clearly higher and are possibly aided by the large stress release on the supershear segment. In other words, in the SZ, the high proportion of aftershocks located off the main fault would exhibit a high b value due to their occurrence on a higher strength material, and the few, which do occur on the main fault, would also show a high b value due to occurrence in the region of the highest stress release. But, as more aftershocks occur off-fault, the former is the dominant controlling feature. This viewpoint seems to be corroborated by the data. But again, whether this *b*-value anomaly is discernible or not depends on the relative values of the average off-fault pre-stress and the strength of the material surrounding the supershear segment in a particular scenario.

A simple check, though not conclusive, of the above hypothesis can be carried out to fur-

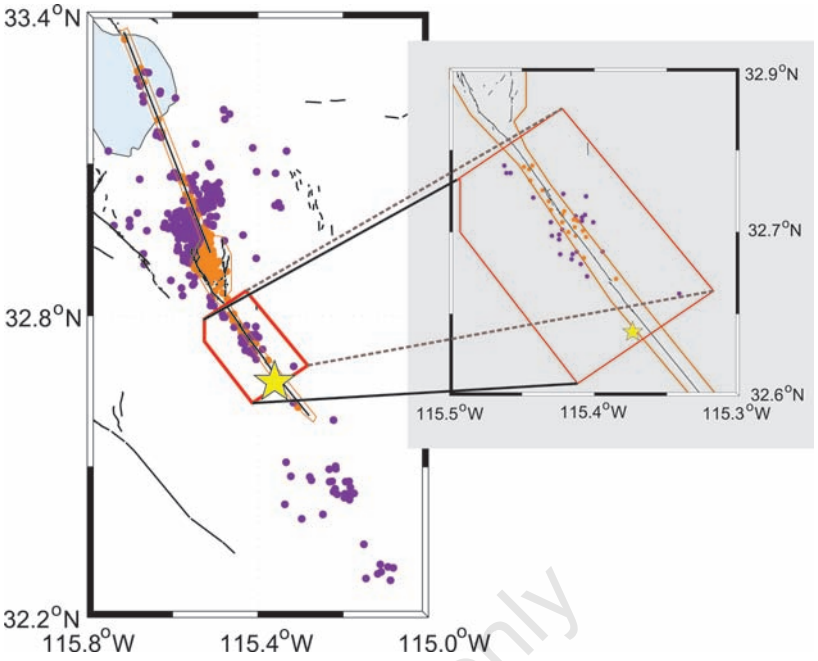


**Figure 7. The narrow zone considered around the rupture for the Imperial Valley sequence. Seismicity inside the zone is shown in orange and events outside the zone in purple. (Left) Map showing the entire rupture. (Right) Enlarged map of only the supershear segment. The *b*-values for both the maps are reported in Table 4. The supershear segment, as before, is shown enclosed in the solid box.**

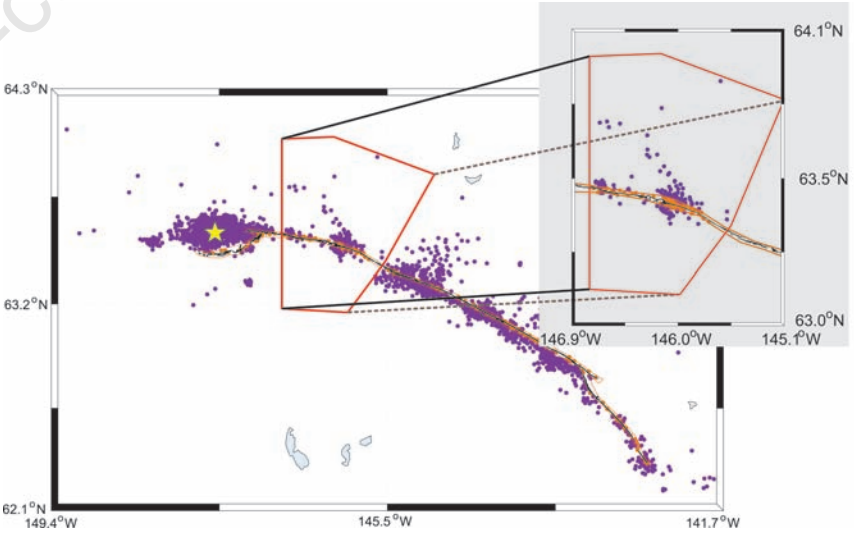


**Figure 8. The narrow zone considered around the rupture for the Denali sequence. The seismicity inside the zone is shown in orange and events outside the zone in purple. (Left) Map showing the entire rupture. (Right) Enlarged of only the supershear segment. The *b*-values for both the maps are reported in Table 4. The supershear segment, as before, is shown enclosed in the solid box.**

ther explore this point. One can compare the aftershocks occurring on the rupture to those occurring away from the main rupture. If the *b*-value anomaly is controlled preferentially by the strength of the material (or the off-fault redistribution) then, in the supershear zone, the *b*-value of off-fault aftershocks should be at least as big (or statistically not significantly smaller) than the *b*-value of the aftershocks that occurred on the rupture. Then, as more off-fault aftershocks occur in the SZ, the strength control should dominate. For the full rupture, however, the *b*-value on and off the fault cannot be compared straight-forwardly due to the local heterogeneities in the *b*-value distribution both on and off the fault. To verify our hypothesis, we undertook the following analysis for the Imperial Valley and Denali sequences. We constructed a very narrow zone (about 0.25 km in half-width) around the surface rupture trace for each of these two events (Figures 7 and 8). We then considered the seismicity inside this zone and calculated the *b*-value (reported as brupt in Table 4). We also considered the seismicity outside this zone (i.e. the rest of the events) and estimate the *b*-value of this subset of magnitudes as well (reported as bout in Table 4). We also ran a significance test of the difference between brupt and bout. Furthermore, we repeated the whole exercise on just the supershear segment of these two ruptures two test our primary hypothesis (Table 4 and Figure 9). We found that the two *b*-values were statistically equivalent at the 95% confidence level both in the SZ as well as for the full rupture. In fact, we observe that bout is systematically larger than brupt in the SZ though this difference is not significant at the 95% level. According to the above discussion, within the SZ, we expected that the *b*-value on the rupture should (at least) not be significantly larger than the *b*-value away from it. This is shown in Table 4 for the supershear zone. However, these statistical results must be treated with caution as such small data sets are not reliable for the purpose of hypothesis testing. The catalogs we use are not relocated and that might affect our hypothesis testing. We also implicitly assume that the *b*-value anomaly is controlled either by the amount of slip or the strength of the material while other effects such as co- or post-seismic pore pressure changes might also affect such anomalies.[49] A high quality, relocated catalog might shed more light on such analysis. Furthermore, the most appropriate analysis would be to use the events exactly on the rupture plane to calculate brupt instead of using aftershocks occurring within a thin zone around the fault trace. But as both faults are nearly vertical in the supershear segment,[23,27] our approximation is acceptable as long as the uncertainties in event locations are smaller than the width of the thin zone around the main fault. In conclusion, the catalogs at our disposal, within their inherent limitations, do support our hypothesis that the off-fault distribution of aftershocks dominantly controls the *b*-value anomaly.

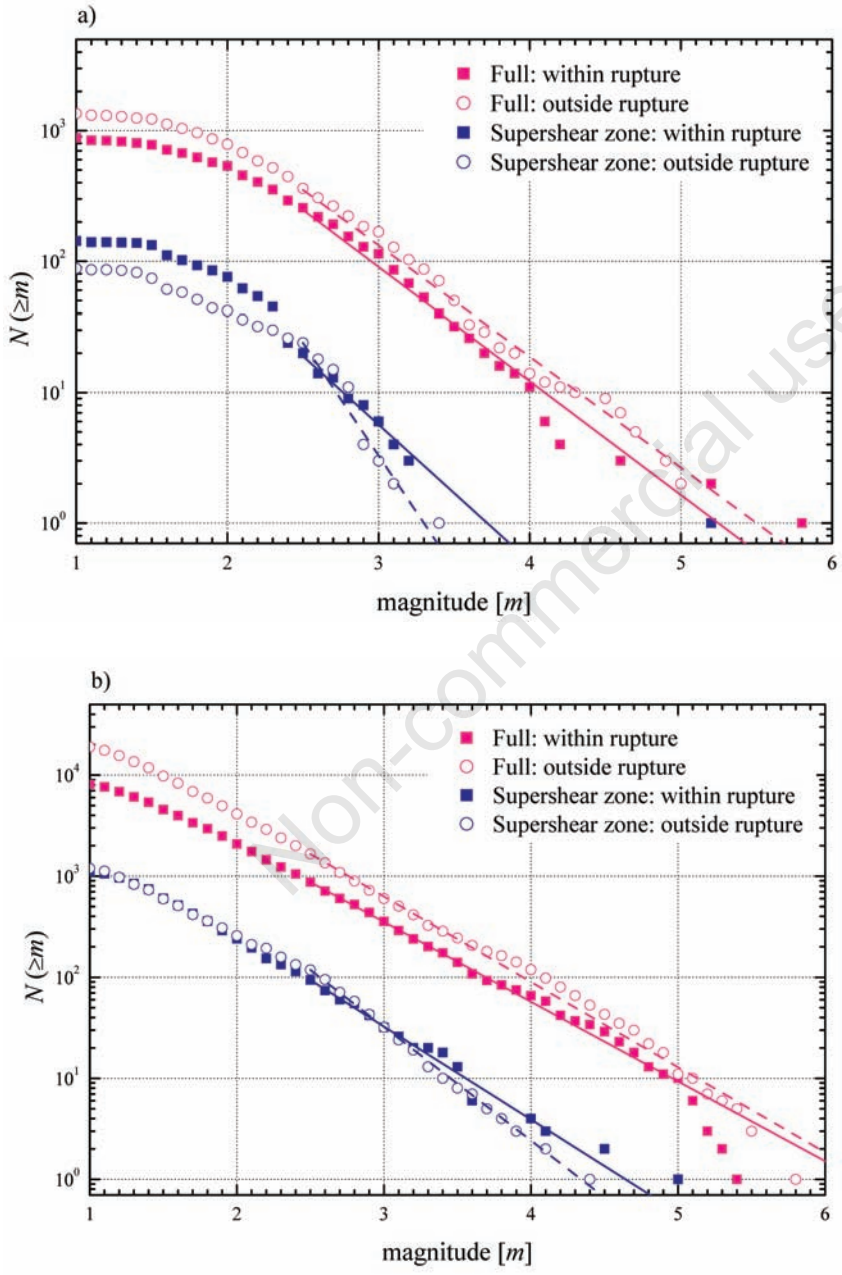


**Figure 9. The frequency-magnitude plots for the populations of aftershocks within (solid symbols) and outside (open symbols) the rupture zone for the full aftershock region (red) and the supershear zone (blue) of (A) the Imperial Valley and (B) the Denali aftershock sequences as considered in the text (see Table 4). The straight lines show the GR law fits for the *b*-values given in Table 4 for the corresponding sequences.**

## The lack of trend in the *p*-value

The reason for the lack of systematic spatial correlation of the *p*-value with the supershear rupture segment is not immediately clear. The mechanism behind the time dependence in Omori law has been debated. Many mechanisms have been proposed for this temporal decay *e.g.* subcritical crack growth,[55] visco-elastic relaxation,[56] post-seismic creep due to stress corrosion in the regions of stress concentration after the mainshock,[57] static fatigue,[58] pore fluid flow,[59] post-seismic slip[60]

and earthquake nucleation under rate- and state-variable friction.[61] Of particular interest to us is the last class of models which simulate aftershocks as seismic events occurring on velocity-weakening nucleation patches obeying a rate-and state-variable friction law triggered to instability by a step stress change due to the occurrence of the mainshock. In the original work, for a uniform stress step (step in time, uniform in space) over all the nucleation patches, it was shown[61] that the decay occurs with a constant $p$=1. Application of spatially heterogeneous step stress changes, instead of spatially uniform step stress changes, on the nucleation patches reveals that the $p$-value increases with increasing heterogeneity in the stress step but never exceeds unity.[62] Additionally, away from the main fault, the $p$-value decreases with offset from the main fault under this framework.[62] The overall Omori exponent might be expected to describe an average rate constructed from a superposition of the rate on the fault and these progressively smaller rates away from the fault. So in the SZ, as the stress release is expected to be only moderately heterogeneous (due to its large magnitude), and as aftershocks are preferentially situated off the fault, we should expect a systematically smaller $p$-value. It is important to note that the requirement of moderate spatial heterogeneity in the stress step in the SZ only ensures that the lowering of the $p$-value due to off-fault aftershocks is not offset by highly heterogeneous stress release. This does not necessarily imply less spatial heterogeneity in the applied stress step in the SZ than the sub-Rayleigh segments. In any case, no such spatial trend in the $p$-value minimum is observed in the $p$-value variations. This could be due to the fact that the stress release from supershear ruptures does not attenuate much with distance away from the fault over length scales of the order of depth of faulting.[22] This is a direct consequence of the generation of shear stress Mach cones over these length scales.[22] The numerical simulations cited above[62,63] impose a decay in the heterogeneous stress step field with distance from the rupture plane in order to observe the smaller aftershock decay rates away from the fault. Therefore, the expectation of smaller $p$-values due to off-fault aftershock distribution may be unreasonable within the SZ. In such a scenario, as we have no clear information about the relative magnitude of the heterogeneity in the imposed stress steps between the supershear and sub-Rayleigh segments, we cannot definitively identify any particular behavior. In other words, one might expect to see no clear trend in the spatial distribution of the $p$-value amongst different mainshocks as the occurrence of the shear mach cone might cancel out the effect of the off-fault aftershock distribution and allow the $p$-value to be controlled by more random physical properties. Also, the rate-and-state-variable framework cannot lead to the p greater than 1 values that we observe (Table 1). There is evidence that such high $p$-values might need other physical controls, such as visco-elastic relaxation or static fatigue,[56,58] and this brings into question the entire line of argument presented above.

## Conclusions

Our analysis describes the relation of the supershear rupture process and the statistics of subsequent aftershocks. We reliably establish that there are statistical anomalies in aftershock sequences of mainshocks associated with the supershear ruptures. The usual assumption of spatial homogeneity of statistical parameters breaks down due to the influence of the rupture process. Such statistical signals can be used to confirm the physical nature of the rupture process. In particular, the spatial maximum of the b value map occurs within the supershear zone. The arguments outlined above point to the fact that the $b$-value anomaly can be related to the occurrence of off-fault aftershocks, which is a signature of supershear ruptures, and seems to point to a strong dependence of the $b$-value to material strength. This finding is, of course, of very wide significance. But our analysis in this regard is based on a simple mathematical model and simplifying physical assumptions and needs to be independently verified. The lack of trend observed in the spatial variation of the $p$-value is much more difficult to understand and no clear physical insight can be developed. The aftershock sequences also seem to yield a slightly smaller (in magnitude) largest aftershock than expected from Båth's Law for the mainshocks of given magnitude. Only detailed numerical or experimental studies probing the basic physics of occurrence of aftershocks can completely describe the physical causes of the statistical anomalies observed here.

## References


1. Mello M, Bhat HS, Rosakis AJ, Kanamori H. Identifying the unique ground motion signatures of supershear earthquakes: Theory and experiments. Tectonophysics 2010;493:297-326.
2. Burridge R. Admissible speeds for plane-strain self-similar shear cracks with friction but lacking cohesion. Geophys J Roy Astron Soc 1973;35:439-55.
3. Andrews DJ. Rupture velocity of plane strain shear cracks. J Geophys Res 1976;81:5679-87.
4. Das S, Aki K. Numerical study of 2-dimensional spontaneous rupture propagation. Geophys J Roy Astron Soc 1977;50:643-68.
5. Archuleta RJ. A faulting model for the 1979 Imperial Valley earthquake. J Geophys Res 1984;89:4559-85.
6. Spudich P, Cranswick E. Direct observation of rupture propagation during the 1979 Imperial Valley earthquake using a short baseline accelerometer array. Bull Seismol Soc Am 1984;74:2083-114.
7. Bouchon M, Toksoz N, Karabulut H, et al. Seismic imaging of the 1999 Izmit (Turkey) rupture inferred from the near-fault recordings. Geophys Res Lett 2000;27:3013-6.
8. Bouchon M, Bouin MP, Karabulut H, et al. How fast is rupture during an earthquake? New insights from the 1999 Turkey earthquakes. Geophys Res Lett 2001;28:2723-6.
9. Bouin MP, Bouchon M, Karabulut H, Aktar M. Rupture process of the 1999 november 12 Duzce (Turkey) earthquake deduced from strong motion and global positioning system measurements. Geophys J Int 2004;159:207-11.
10. Konca AO, Leprince S, Avouac JP, Helmberger DV. Rupture process of the 1999 m-w7.1 Duzce earthquake from joint analysis of SPOT, GPS, InSAR, Strong-Motion, and Teleseismic data: A supershear rupture with variable rupture velocity. Bull Seismol Soc Am 2010;100:267-88.
11. Bouchon M, Vallee M. Observation of long supershear rupture during the magnitude 8.1 Kunlunshan earthquake. Science 2003;301:824-6.
12. Robinson DP, Brough C, Das S. The Mw 7.8, 2001 Kunlunshan earthquake: Extreme rupture speed variability and effect of fault geometry. J Geophys Res 2006;111:B08303.
13. Vallee M, Landes M, Shapiro NM, Klinger Y. The 14 November 2001 Kokoxili (Tibet) earthquake: High-frequency seismic radiation originating from the transitions between sub-Rayleigh and supershear rupture velocity regimes. J Geophys Res2008;113:B07305.
14. Aagaard BT, Anderson G, Hudnut KW. Dynamic rupture modeling of the transition from thrust to strike-slip motion in the 2002 Denali fault earthquake, Alaska. Bull Seismol Soc Am 2004;94:S190-201.
15. Dunham EM, Archuleta RJ. Evidence for a supershear transient during the 2002 Denali fault earthquake. Bull Seismol Soc Am 2004;94:S256-68.
16. Ellsworth WL, Celebi M, Evans JR, et al. Near-Field ground motion of the 2002 Denali fault, Alaska, earthquake recorded at pump station 10. Earthq Spectra 2004;20:597-615.

17. Olsen KB, Madariaga R, Archuleta RJ. Three-dimensional dynamic simulation of the 1992 Landers earthquake. Science 1997;278:834-8.
18. Peyrat S, Olsen K, Madariaga R. Dynamic modeling of the 1992 Landers earthquake. J Geophys Res 2001;106:26467-82.
19. Rosakis AJ. Intersonic shear cracks and fault ruptures. Adv Phys 2002;51:1189-257.
20. Dunham EM. Conditions governing the occurrence of supershear ruptures under slip-weakening friction. J Geophys Res 2007;112:B07302.
21. Lu X, Lapusta N, Rosakis AJ. Analysis of supershear transition regimes in rupture experiments: the effect of nucleation conditions and friction parameters. Geophys J Int 2009;177:717-32.
22. Bhat HS, Dmowska R, King GCP, et al. Off-fault damage patterns due to supershear ruptures with application to the 2001 mw 8.1 Kokoxili (Kunlun) Tibet earthquake. J Geophys Res 2007;112:B06301.
23. Bouchon M, Karabulut H. The aftershock signature of supershear earthquakes. Science 2008;320:1323-5.
24. Rosakis AJ, Samudrala O, Coker D. Cracks faster than the shear wave speed. Science 1999;284:1337-40.
25. Xia KW, Rosakis AJ, Kanamori H. Laboratory earthquakes: The sub-rayleigh-to supershear rupture transition. Science 2004;303:1859-61.
26. Xia KW, Rosakis AJ, Kanamori H, Rice JR. Laboratory earthquakes along inhomogeneous faults: Directionality and supershear. Science 2005;308:681-4.
27. Bouchon M, Karabulut H, Bouin MP, et al. Faulting characteristics of supershear earthquakes. Tectonophysics 2010;493: 244-53.
28. Dunham EM, Favreau P, Carlson JM. A supershear transition mechanism for cracks. Science 2003;299:1557-9.
29. Dunham EM, Bhat HS. Attenuation of radiated ground motion and stresses from three-dimensional supershear ruptures. J Geophys Res 2008;113:B08319.
30. Aki K. Asperities, barriers, characteristic earthquakes and strong motion prediction. JGeophys Res 1984;89:5867-72.
31. Sharp RV, Lienkaemper JJ, Bonilla MG, et al. Surface faulting in the central Imperial Valley. The Imperial Valley, California, earthquake of October 15, 1979. In: US Prof. Paper 1254, 1982. pp. 119-43.
32. Eberhart-Phillips D, Haeussler PJ, et al. The 2002 Denali fault earthquake, Alaska: A large magnitude, slip-partitioned event. Science 2003;300:1113-8.
33. Oglesby DD, Dreger DS, Harris RA, et al. Inverse kinematic and forward dynamic models of the 2002 Denali fault earthquake, Alaska. Bull Seismol Soc Am 2004;94:S214-S233.
34. Gutenberg B, Richter CF. Frequency of earthquakes in California. Bull Seismol Soc Am 1944;34:185-8.
35. Utsu T. A statistical study on the occurrence of aftershocks. Geophys Mag 1961;30:521-605.
36. Båth M. Lateral inhomogeneities in the upper mantle. Tectonophysics 1965;2:483-514.
37. Aki K. Maximum likelihood estimate of b in the formula logN = a - bM and its confidence limits. Bull Earthquake Res Inst Tokyo Univ 1965;43:237-9.
38. Utsu T. A method for determining the value of b in a formula log n = a - bM showing the magnitude-frequency relation for earthquakes. Geophys Bull Hokkaido Univ 1965;13:99-103.
39. Bender B. Maximum-likelihood estimation of b-values for magnitude grouped data. Bull Seismol Soc Am 1983;73:831-51.
40. Tinti S, Mulargia F. Confidence intervals of b-values for grouped magnitudes. Bull Seismol Soc Am 1987;77:2125-34.
41. Guttorp P, Hopkins D. On estimating varying b-values. Bull Seismol Soc Am 1986;76:889-95.
42. Woessner J, Wiemer S. Assessing the quality of earthquake catalogues: Estimating the magnitude of completeness and its uncertainty. Bull Seismol Soc Am 2005;95:684-98.
43. Utsu T, Ogata Y, Matsuura RS. The centenary of the Omori formula for a decay law of aftershock activity. J Phys Earth 1995;43:1-33.
44. Guo ZQ, Ogata Y. Statistical relations between the parameters of aftershocks in time, space, and magnitude. J Geophys Res 1997;102:2857-73.
45. Shcherbakov R, Turcotte DL. A modified form of Bath's law. Bull Seismol Soc Am. 2004;94:1968-75.
46. Peng ZG, Vidale JE, Houston H. Anomalous early aftershock decay rate of the 2004 Mw 6.0 Parkfield, California, earthquake. Geophys Res Lett 2006;33:L17307.
47. Peng ZG, Vidale JE, Ishii M, Helmstetter A. Seismicity rate immediately before and after main shock rupture from high-frequency waveforms in Japan. J Geophys Res 2007;112:B03306.
48. Amorese D, Grasso JR, Rydelek PA. On varying b-values with depth: results from computer-intensive tests for Southern California. Geophys J Int 2010;180:347-60.
49. Wiemer S, Katsumata K. Spatial variability of seismicity parameters in aftershock zones. J Geophys Res 1999;104:13135-51.
50. Scholz CH. The frequency-magnitude relation of microfracturing in rock and its relation to earthquakes. Bull Seismol Soc Am 1968;58:399-415.
51. Mogi K. Study of elastic shocks caused by the fracture of hetergeneous materials and its relations to earthquake phenomena. Bull Earthquake Res Inst 1962;40:125-73.
52. Mori J, Abercrombie RE. Depth dependence of earthquake frequency-magnitude distributions in California: Implications for rupture initiation. J Geophys Res 1997;102:15081-90.
53. Schorlemmer D, Wiemer S, Wyss M. Variations in earthquake-size distribution across different stress regimes. Nature 2005;437:539-42.
54. Gerstenberger M, Wiemer S, Giardini D. A systematic test of the hypothesis that the b value varies with depth in California. Geophys Res Lett 2001;28:5760.
55. Das S, Scholz CH. Theory of time-dependent rupture in the earth. J Geophys Res 1981;86:6039-51.
56. Mikumo T, Miyatake T. Earthquake sequences on a frictional fault model with non- uniform strengths and relaxation times. Geophys J R Astron Soc 1979;59: 497-522.
57. Scholz CH. Microfractures, aftershocks, and seismicity. Bull Seismol Soc Am 1968;58:1117-30.
58. Narteau C, Shebalin P, Holschneider M. Temporal limits of the power law aftershock decay rate. J Geophys Res 2002;107: 2359.
59. Nur A, Booker JR. Aftershocks caused by pore fluid pressure? Science 1971;175:885-7.
60. Schaff DP, Beroza GC, Shaw BE. Postseismic response of repeating aftershocks. Geophys Res Lett 1998;25:4549-52.
61. Dieterich J. A constitutive law for rate of earthquake production and its application to earthquake clustering. J Geophys Res 1994;99:2601-18.
62. Helmstetter A, Shaw BE. Relation between stress heterogeneity and aftershock rate in the rate-and-state model. J Geophys Res 2006;111:B07304.
63. Marsan D. Can coseismic stress variability suppress seismicity shadows? Insights from a rate-and-state friction model. J Geophys Res 2006;111:B06305.